Nuclear Materials and Energy 42 (2025) 101887

Contents lists available at ScienceDirect

Nuclear Materials and Energy

journal homepage: www.elsevier.com/locate/nme

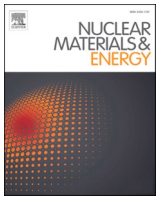

Improved Coulomb collision operator for kinetic ion transport with EMC3-EIRENE simulating Nitrogen seeding in medium density ITER L-mode scenario☆

D. Harting [a,*], D. Reiser [a], S. Rode [a], J. Romazanov [a], P. Börner [a], Y. Feng [b], H. Frerichs [c], A. Knieps [a]

[a] Forschungszentrum Jülich GmbH, Institut für Energie– und Klimaforschung – Plasmaphysik, Partner of the Trilateral Euregio Cluster (TEC) 52425 Jülich, Germany
[b] Max Planck Institute for Plasma Physics 17491 Greifswald, Germany
[c] University of Wisconsin– Madison, Department of Engineering Physics, WI, USA

ARTICLE INFO

Keywords:
EMC3-EIRENE
Kinetic ion transport simulation
Coulomb collision model
Adaptive time step control with error estimate
Scrape of layer modeling

ABSTRACT

Previous simulations with the kinetic ion transport module of EMC3-EIRENE for Nitrogen seeding in a medium density ITER L-mode scenario showed that the currently simplified Coulomb collision model of EIRENE leads to a strongly overestimated confinement of the kinetic ions in the magnetic mirror regions. This simplified Coulomb collision model in EIRENE is based on an energy relaxation time only and is not changing the ratio of the parallel and perpendicular velocity components for the kinetic ions and thus does not include any scattering of the kinetic ions into the loss cone of the magnetic mirror. We have now implemented a new Coulomb collision operator in EIRENE, where the Coulomb collisions are described by a linear kinetic equation in Fokker-Planck form utilizing the Trubnikov-Rosenbluth potential functions, which includes scattering of the kinetic ions as well as friction with the background plasma. The Fokker-Planck equation is treated by an operator splitting scheme and is solved locally by a Monte-Carlo method. The choice of a small enough time step in the Monte-Carlo integration method is crucial and depends strongly on the local plasma background. Two methods to locally adapt the Monte-Carlo integration time step were implemented. One uses simply a fraction ($\sim 10^{-4}$) of the local Spitzer slowing down time and the other applies an adaptive time step control with error estimation. It turns out that simulations using the adaptive time step control method are up to a factor 10 faster compared to the time step control using the Spitzer slowing down time. In this work we will present the details of this newly implemented Coulomb collision operator for kinetic ions in EMC3-EIRENE and the implementation of the adaptive time step algorithm. We applied this new Coulomb collision operator in a kinetic ion simulation with EMC3-EIRENE for Nitrogen seeding, where we puffed Nitrogen from the top of the machine in an attached medium density ITER L-mode scenario ($n_{sep} = 1\times10^{19}$ m^{-3}, $P_{sep} = 20$ MW). This shows that the unphysical and exaggerated confinement of the kinetic ions in the magnetic mirror regions observed with the simplified Coulomb collision model in EIRENE is now resolved with the new Coulomb collision operator, which treats the scattering of the kinetic ions into the loss cone of the magnetic mirror correctly.

1. Introduction

Previous simulations with the kinetic ion transport module of EMC3-EIRENE [1–3] for Nitrogen seeding in a medium density ITER L-mode scenario showed that the currently simplified Coulomb collision model of EIRENE leads to a strongly overestimated confinement of the kinetic ions in the magnetic mirror regions [4]. This simplified Coulomb collision model in EIRENE is based on an energy relaxation time only and is not changing the ratio of the parallel and perpendicular velocity components for the kinetic ions and thus does not include any scattering of the kinetic ions into the loss cone of the magnetic mirror.

We have now implemented a new Coulomb collision operator in EIRENE based on [5], where the Coulomb collisions are described by a linear kinetic equation in Fokker-Planck form utilizing the Trubnikov-

☆ This article is part of a special issue entitled: 'PSI-26' published in Nuclear Materials and Energy.

* Corresponding author.
E-mail address: d.harting@fz-juelich.de (D. Harting).

https://doi.org/10.1016/j.nme.2025.101887
Received 5 July 2024; Received in revised form 20 December 2024; Accepted 27 January 2025
Available online 11 February 2025

Rosenbluth potential functions, which includes scattering of the kinetic ions as well as friction with the background plasma. The Fokker-Planck equation for the Coulomb collisions is treated by an operator splitting scheme and is solved locally by a Monte-Carlo method in velocity space.

In this work we will present the details of this newly implemented Coulomb collision operator for kinetic ions in EIRENE and the implementation of an adaptive time step algorithm with error estimate base on the work in [6,7] to ensure convergence of the Monte-Carlo method for the Coulomb collisions in velocity space. We applied this new Coulomb collision operator in a kinetic ion simulation with EMC3-EIRENE for Nitrogen seeding to the same conditions as in [4], where we puffed Nitrogen from the top of the machine in an attached medium density ITER L-mode scenario ($n_{sep} = 1 \times 10^{19}\,\mathrm{m}^{-3}$, $P_{sep} = 20$ MW). This shows that the unphysical and exaggerated confinement of the kinetic ions in the magnetic mirror regions observed with the simplified Coulomb collision model in EIRENE [4] is now resolved with the new Coulomb collision operator, which treats the scattering of the kinetic ions into the loss cone of the magnetic mirror correctly. Finally, we will present also a first comparison of the EMC3-EIRENE kinetic ion transport module with the well-established ERO2.0 code on an artificial Beryllium transport simulation.

2. Improved Coulomb collision operator

The kinetic ion transport model in EMC3-EIRENE is based on a guiding centre model in trace ion approximation and is solved by a Monte-Carlo method in real space. The verification of the fundamental transport properties of the model was shown already in [4]. Currently, the EMC3 code includes only an approximated parallel electric field based on a simplified momentum balance for the electrons. For this reason, we are currently not taking into account any $\vec{E} \times \vec{B}$ drift or acceleration of the kinetic ions in the electric field. The Monte-Carlo step of the EMC3-EIRENE kinetic ion transport model is then given by the following equation:

$$\Delta\vec{R}_{gc} = \vec{V}_{gc}\Delta t_{gc} + \sqrt{4D_\perp \Delta t_{gc}}\ \vec{\xi}_\perp \tag{1}$$

Where $D_\perp$ is the diffusion coefficient representing the anomalous perpendicular transport, $\vec{\xi}_\perp$ is a random unit vector perpendicular to the magnetic field and Δt_{gc} is the time step of the Monte-Carlo scheme in real space. The guiding centre velocity $\vec{V}_{gc}$ is given by the equation

$$\vec{V}_{gc} = v_\parallel \frac{\vec{B}}{B} + \frac{v_\parallel^2 + \frac{v_\perp^2}{2}}{\frac{qB}{m}} \frac{\vec{B}\times\vec{\nabla}B}{B^2} \tag{2}$$

with

$$\Delta v_\parallel = -\frac{v_\perp^2}{2}\frac{\nabla_\parallel B}{B}\Delta t_{gc} + \Delta v_{\parallel,cc} \tag{3}$$

$$\Delta v_\perp = \frac{v_\parallel v_\perp}{2}\frac{\nabla_\parallel B}{B}\Delta t_{gc} + \Delta v_{\perp,cc} \tag{4}$$

and q and m being the charge and mass of the kinetic ions. Here the terms $\Delta v_{\parallel,cc}$ and $\Delta v_{\perp,cc}$ represent the contributions from the new Coulomb collision operator based on the work presented in [5] over the duration of the guiding centre time step Δt_{gc}.

So far, the EIRENE code has treated impurity ions in a simplified way by energy relaxation, but without considering in detail the Coulomb collisions with a Maxwellian background (as assumed in EMC3). The implementation presented here is based on the test particle approach, which assumes that impurities change their velocity distribution due to collisions with the background plasma, but that the background is not changed by Coulomb collisions with the test particles (although it could be changed by radiation processes and particle sources and sinks, which could be taken into account in the iterative coupling of EMC3 and EIRENE). The Coulomb collision operator of our model has already been discussed in detail in references [5,6] and [8]. Here, we would like to emphasize once again that we restrict ourselves to collisions with a Maxwell-distributed background. For a more general situation, e.g. with arbitrary velocity distributions of the background, more sophisticated methods for simulating Coulomb collisions would have to be used (see, for example [9–11]). We would like to stress once more that our model is based on the assumption that the kinetic impurities are considered as test particles, which means that the Coloumb collisions in our simulations are not completely consistent. The test particles undergo a relaxation process, but they are assumed not to change background temperature and momentum via Coulomb collisions.

The form of the drift $\vec{\mathscr{K}}$ and diffusion coefficients $\overline{\overline{\mathscr{D}}}$ for the Coulomb collisions in [5] and [8] is derived along the so-called Itô approach [12] which means that in a general coordinate system the Fokker-Planck equation for the probability function $f(\vec{x})$

$$\frac{\partial f}{\partial t} = -\vec{\nabla}\cdot\left[\vec{\mathscr{K}}f - \frac{1}{2}\vec{\nabla}\cdot(\overline{\overline{\mathscr{D}}}f)\right] \tag{5}$$

corresponds to the following stochastic differential equations for each component of $\vec{x}$

$$dx_i = \left(\mathscr{K}^i - \frac{1}{2}\Gamma^i_{jk}\mathscr{D}^{jk}\right)dt \ + \ \vec{e}^{\,i}\cdot\overline{\overline{\sigma}}\cdot d\vec{W} \tag{6}$$

written in co– and contravariant components with base vectors $\vec{e}^{\,i}$, Christoffel symbols Γ^i_{jk} and $\overline{\overline{\sigma}}\cdot\overline{\overline{\sigma}}^T = \overline{\overline{\mathscr{D}}}$.

With this the contributions $\Delta v_{\parallel,cc}$ and $\Delta v_{\perp,cc}$ in equations (3) and (4) from the Coulomb collisions to each guiding centre step can be simulated by a Monte-Carlo scheme in velocity space which divides the guiding centre time step in N steps with smaller time steps Δt^k_{cc} so that $\Delta t_{gc} = \sum_{k=1}^N \Delta t^k_{cc}$ and $\Delta v_{\parallel,cc} = \sum_{k=1}^N \Delta v^k_{\parallel,cc}$ as well as $\Delta v_{\perp,cc} = \sum_{k=1}^N \Delta v^k_{\perp,cc}$. The individual changes of the parallel and perpendicular velocity components $\Delta v^k_{\parallel,cc}$ and $\Delta v^k_{\perp,cc}$ over the time step Δt^k_{cc} are given by

$$\begin{aligned}\Delta v^k_{\parallel,cc} \ = \ & -\left(1+\frac{m}{m_B}\right)\frac{\mathfrak{D}_\parallel \chi_\parallel}{u_B}\Delta t^k_{cc} \\ & + \ \xi_1\frac{\chi_\parallel}{\chi}\sqrt{\mathfrak{D}_\parallel \Delta t^k_{cc}} \ - \ \xi_2\frac{\chi_\perp}{\chi}\sqrt{\mathfrak{D}_\perp \Delta t^k_{cc}}\end{aligned} \tag{7}$$

$$\begin{aligned}\Delta v^k_{\perp,cc} \ = \ & \left[-\left(1+\frac{m}{m_B}\right)\frac{\mathfrak{D}_\parallel \chi_\perp}{u_B} + \frac{1}{2}\frac{\mathfrak{D}_\perp}{v_\perp}\right]\Delta t^k_{cc} \\ & + \ \xi_1\frac{\chi_\perp}{\chi}\sqrt{\mathfrak{D}_\parallel \Delta t^k_{cc}} \ + \ \xi_2\frac{\chi_\parallel}{\chi}\sqrt{\mathfrak{D}_\perp \Delta t^k_{cc}}\end{aligned} \tag{8}$$

with ξ_1, ξ_2 being normal distributed random numbers. The coefficients above can all be calculated from the given plasma background parameters like ion density (n_B), temperature ($T_{i,B}$) and parallel streaming velocity ($V_{\parallel,B}$).

$$\chi_\perp = \frac{v_\perp}{u_B}; \qquad \chi_\parallel = \frac{v_\parallel - V_{\parallel,B}}{u_B}; \qquad \chi = \sqrt{{\chi_\perp}^2 + {\chi_\parallel}^2} \tag{9}$$

$$u_B = \sqrt{\frac{2k_b T_{i,B}}{m_B}}; \qquad \Lambda = \frac{Z^2 Z_B^2 e^4 n_B \ln(\lambda)}{4\pi\varepsilon_0^2 m^2} \tag{10}$$

$$\mathfrak{D}_\parallel = \frac{\Lambda}{u_B}\left(\frac{\Phi(\chi)}{\chi^3} - \frac{\Phi'(\chi)}{\chi^2}\right); \qquad \mathfrak{D}_\perp = \frac{\Lambda}{u_B}\left(\frac{\Phi'(\chi)}{2\chi^2} + \frac{\Phi(\chi)}{\chi} - \frac{\Phi(\chi)}{2\chi^3}\right) \tag{11}$$

$$\Phi(\chi) = \mathrm{erf}(\chi); \qquad \Phi'(\chi) = \frac{2}{\sqrt{\pi}}e^{-\chi^2} \tag{12}$$

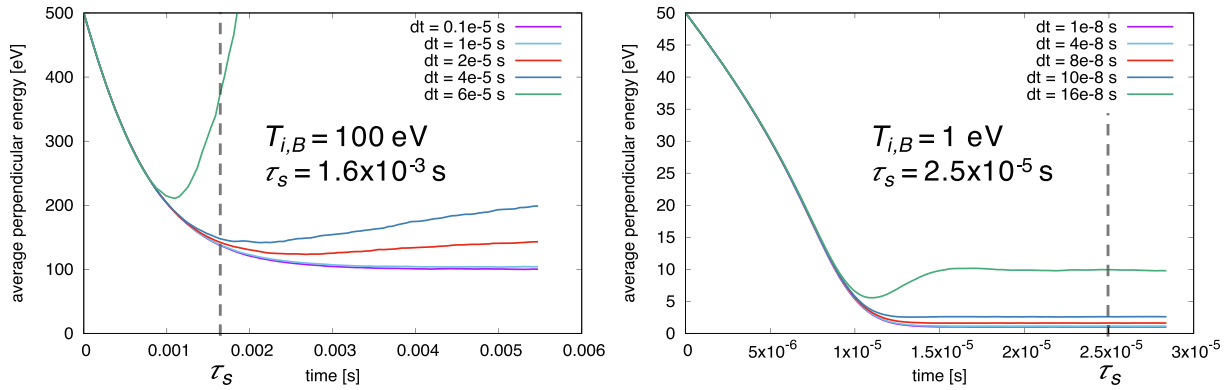

Fig. 1. Relaxation of the average perpendicular energy of an ensemble of MC-particles for different MC time steps into a plasma background with an ion temperature of 100 eV (left figure) and 1 eV (right figure).

Where m_B and Z_B are the mass and charge number of the plasma background ions, m and Z are the mass and charge number of the kinetic test ions and $\ln(\lambda)$ is the Coulomb logarithm (currently set fixed to 13.5 in EIRENE). This Coulomb collision operator is valid only for unperturbed Maxwellian velocity distributions of the background plasma and thus neglects any thermal force effects arising from the parallel temperature gradient of the background plasma. We plan to include the thermal force effect in future updates to the Coulomb collision operator.

It is crucial that the time steps Δt^k_{cc} from equations (7) and (8) are small enough, otherwise the contribution from the coulomb collisions diverges. This is illustrated in Fig. 1 where the relaxation of the average perpendicular energy of an ensemble of 10^6 Monte-Carlo particles towards a constant background plasma ($n_B = 10^{19}$ m^{-3} and $T_{i,B} = 100$ eV on left plot, $T_{i,B} = 1$ eV on right plot) is shown for different time steps Δt^k_{cc}. In the left plot of Fig. 1, the Monte-Carlo particles start with a mono energetic distribution of $v_\parallel = v_\perp = 500$ eV and in the right plot of $v_\parallel = v_\perp = 50$ eV. The Coulomb collisions should then relax the velocity distribution of the Monte-Carlo particles to a Maxwellian velocity distribution with the background plasma temperature $T_{i,B} = 100$ eV in the left plot and $T_{i,B} = 1$ eV in the right plot. This is well achieved for $\Delta t^k_{cc} = 10^{-6}$ s in the left plot and $\Delta t^k_{cc} = 10^{-8}$ s in the right plot. But when the time step becomes larger, the final velocity distributions get distorted and the results start to diverge. A simple estimate for the time step Δt^k_{cc} can be obtained by using a small fraction (typically 10^{-4}) from the Spitzer slowing down time $\tau_s = \left[\left(1+\frac{m}{m_B}\right)\frac{\mathfrak{D}_\parallel}{u_B^2}\right]^{-1}$, but this is not effective enough over the large possible plasma background temperature range (0.1 eV – 1000 eV) in the simulation volume. For this reason, we have implemented an adaptive time step control with error estimate for the Monte-Carlo scheme of the Coulomb collision.

3. Adaptive time step control

The adaptive time step control with error estimate implemented for the new Coulomb collision operator in EMC3-EIRENE is based on the adaptive time step control presented in [6,7] and was slightly adapted in the definition of ε_{drift} and ε_{diff} in equations (16) and (17) for the current needs. The equations (7) and (8) are of the form:

$$\Delta v_\parallel = \alpha_1(v_\parallel, v_\perp)\Delta t + \xi_1\alpha_2(v_\parallel, v_\perp)\sqrt{\Delta t} - \xi_2\alpha_3(v_\parallel, v_\perp)\sqrt{\Delta t} \tag{13}$$

$$\Delta v_\perp = \alpha_4(v_\parallel, v_\perp)\Delta t + \xi_1\alpha_5(v_\parallel, v_\perp)\sqrt{\Delta t} + \xi_2\alpha_6(v_\parallel, v_\perp)\sqrt{\Delta t} \tag{14}$$

With a given tolerance $\varepsilon_{tol} \sim 10^{-4}$ we can define an absolute tolerable error for the Monte-Carlo step by:

$$\varepsilon_{abs} = \varepsilon_{tol}\sqrt{\left(|\alpha_1|\Delta t + (|\alpha_2| + |\alpha_3|)\sqrt{\Delta t}\right)^2 + \left(|\alpha_4|\Delta t + (|\alpha_5| + |\alpha_6|)\sqrt{\Delta t}\right)^2} \tag{15}$$

We can further define error controls ε_{drift} for the deterministic parts of equations (13) and (14) and ε_{diff} for the stochastic parts by:

$$\varepsilon_{drift} = \frac{(\Delta t)^2}{2\varepsilon_{abs}}\max\left\{\left|\alpha_1\frac{\partial\alpha_1}{\partial v_\parallel}\right|,\ \left|\alpha_4\frac{\partial\alpha_4}{\partial v_\perp}\right|\right\} \tag{16}$$

$$\varepsilon_{diff} = \frac{(\Delta t)^{3/2}}{6\varepsilon_{abs}}\max\left\{\left|\alpha_2\left(\frac{\partial\alpha_2}{\partial v_\parallel}\right)^2\right|,\ \left|\alpha_3\left(\frac{\partial\alpha_3}{\partial v_\parallel}\right)^2\right|,\ \left|\alpha_5\left(\frac{\partial\alpha_5}{\partial v_\perp}\right)^2\right|,\ \left|\alpha_6\left(\frac{\partial\alpha_6}{\partial v_\perp}\right)^2\right|\right\} \tag{17}$$

A time step Δt can now be accepted if $\varepsilon_{drift} < 1$ and $\varepsilon_{diff} < 1$, otherwise the time step is rejected and the Monte-Carlo step is repeated. Whatever if the time step was accepted or rejected, the time step Δt is adapted at the next or repeated Monte-Carlo step. The choice of the next (adapted) time step depends on whether or not the current equations (13) and (14) are diffusion or drift dominated. First of all, we define an estimate for an "optimal" time step

$$\Delta t^* = \left(\beta\varepsilon_{diff}^{-\frac{1}{3}}\sqrt{\Delta t}\right)^2 \tag{18}$$

where $\beta < 1$ is a safety factor (e.g. $\beta = 0.9$).

Weak diffusion: $\varepsilon_{drift} > \varepsilon_{diff}$

In the case of weak diffusion ($\varepsilon_{drift} > \varepsilon_{diff}$) we define the next adapted time step by

$$\Delta t_{next} = j\frac{\Delta t^*}{3} \tag{19}$$

where $\Delta t^* = \min\left\{1.5, \beta\varepsilon_{drift}^{-1/2}\right\}\Delta t$ and $j = \max\left\{j = 1\cdots3 \text{ with } j\frac{\Delta t^*}{3} < \Delta t^*\right\}$.

Diffusion dominated: $\varepsilon_{diff} > \varepsilon_{drift}$

In the diffusion dominated regime ($\varepsilon_{diff} > \varepsilon_{drift}$) the next adapted time step is given in a similar way by

$$\Delta t_{next} = i\frac{\Delta t}{3} \tag{20}$$

which uses the previous time step Δt directly and $i = \max\left\{i = 1\cdots I_{max} \text{ with } i\frac{\Delta t}{3} < \Delta t^*\right\}$ where I_{max} depends on whether the previous time

Table 1
Molecular processes of the AMJUEL database used for Nitrogen molecules N_2 and molecular ions N_2^+ in the simulation.

AMJUEL 2.7.5:	$e + N_2 \rightarrow e + N + N$
AMJUEL 2.7.9:	$e + N_2 \rightarrow e + N_2^+ + e$
AMJUEL 2.7.10:	$e + N_2 \rightarrow e + N + N^+ + e$
AMJUEL 2.7.11:	$e + N_2^+ \rightarrow e + 2N^+ + e$
AMJUEL 2.7.12:	$e + N_2^+ \rightarrow e + N + N^+ + e$

step was accepted or rejected.

$$I_{max} = \begin{cases} 6 : \text{if } \Delta t \text{ was accepted} \\ 2 : \text{if } \Delta t \text{ was rejected} \end{cases} \quad (21)$$

It has turned out that applying this adaptive time step algorithm is up to 10 times faster than the simple method by limiting the time step by a fraction (10^{-4} s) of the Spitzer slowing down time τ_s.

4. Simulations of Nitrogen seeding

With the new and improved coulomb collision operator we repeat now the simulation of Nitrogen seeding in a medium density (attached) ITER L-mode background plasma shown in [4] with a separatrix density of $n_{sep} = 1 \times 10^{19}$ m^{-3} and $P_{sep} = 20$ MW heating power crossing the separatrix from the core. In this plasma background we puff Nitrogen molecules from the top of the machine with a puff strength of $\Gamma_{puff} = 1 \times 10^{18}$ s^{-1} and an energy of 0.026 eV. The perpendicular anomalous diffusion coefficient $D_\perp$ for the kinetic ions was set to 0.3 m^2/s. We use ADAS 96 [13] ionization and recombination rates for atomic Nitrogen and all ionization stages together with the AMJUEL [14] data for the molecular processes listed in Table 1.

The simulation results with the improved Coulomb collision operator

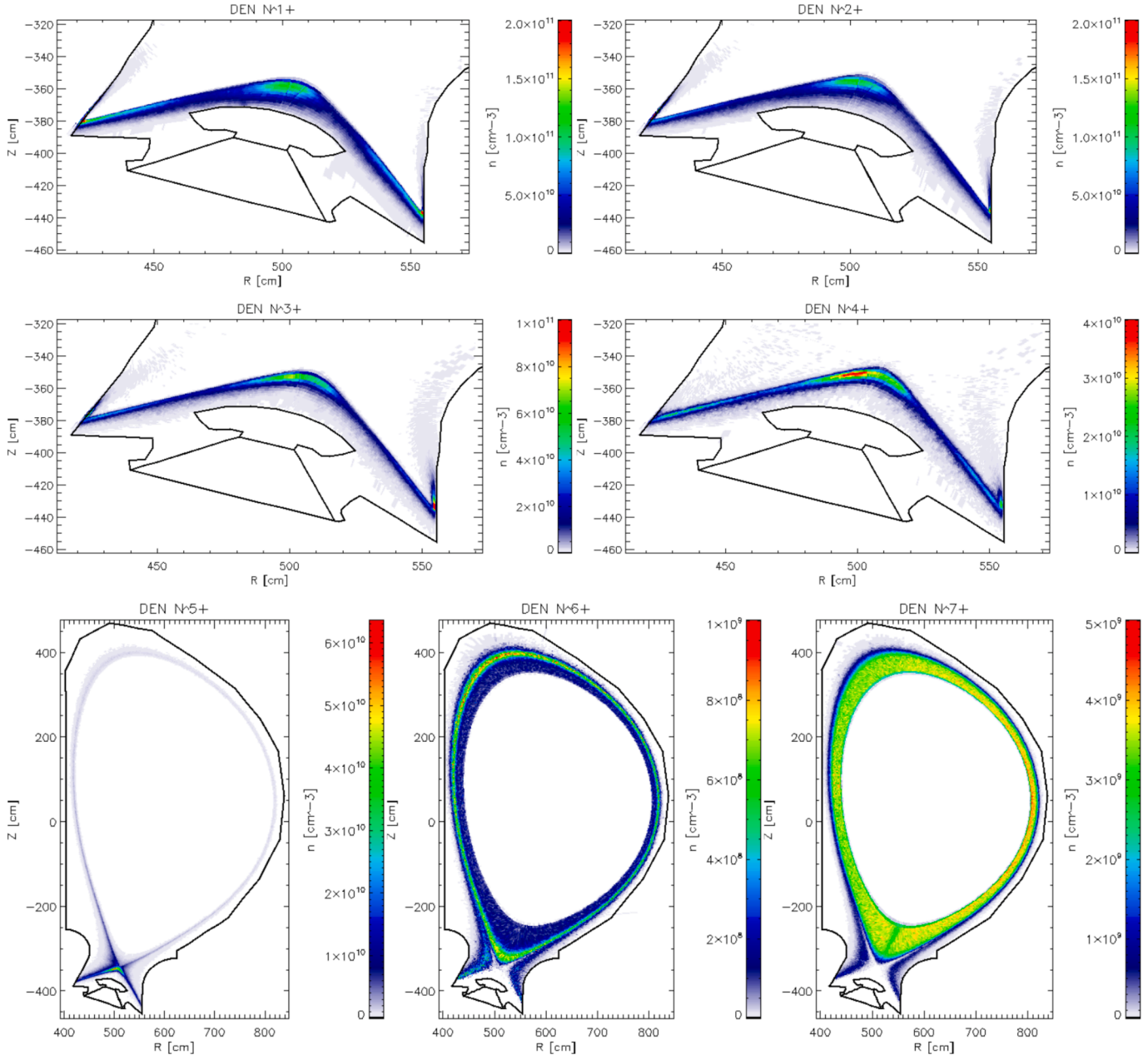

Fig. 2. Simulation results of the EMC3-EIRENE kinetic ion transport module with the improved Coulomb collision operator. Density profiles of the seven different ionization stages of Nitrogen puffed in a medium density ITER L-mode background plasma.

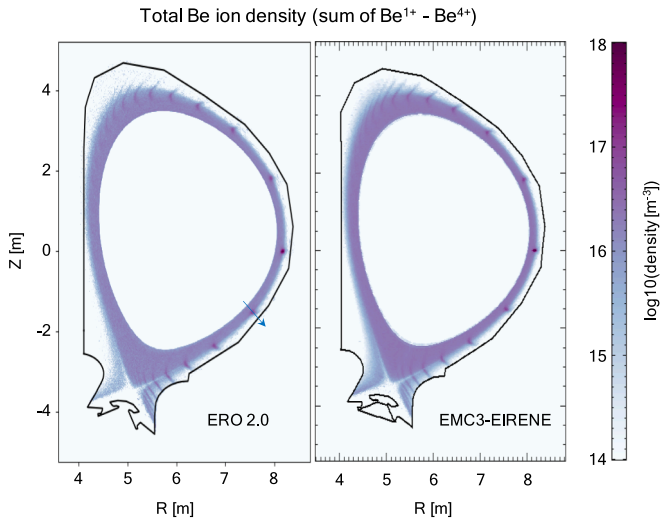

Fig. 3. Total Beryllium ion density at $\varphi = 0^{\circ}$ of an artificial Beryllium puff located at the outer midplane simulated by the ERO2.0 code and the EMC3-EIRENE kinetic ion transport module. The simulation volume has a 40° toroidal symmetry and the ITER background plasma is the same as in section 4.

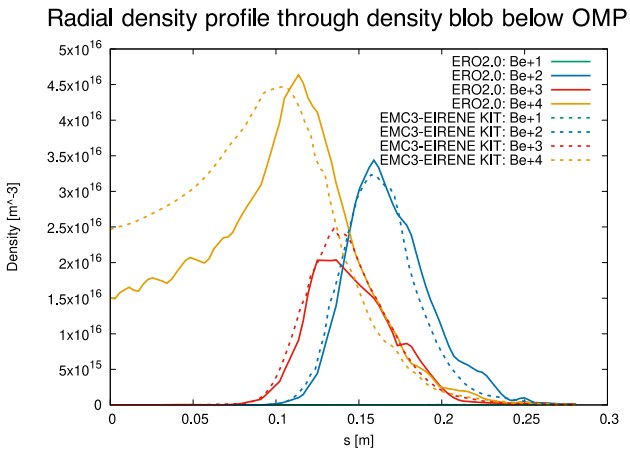

Fig. 4. Radial (going outward) density profiles through the density blob below the outer midplane for the first four ionization stages of Beryllium obtained by the ERO2.0 (solid lines) code and EMC3-EIRENE (dashed lines) kinetic ion transport module (KIT). The location of the radial profile is show in Fig. 3 on the left plot by the blue arrow.

of the EMC3-EIRENE kinetic ion transport module (KIT) are shown in Fig. 2. One can see that the first four ionization stages $N^{1+} - N^{4+}$ of Nitrogen are mainly located in the divertor region. Only the fifth ionization stage N^{5+} starts leaking out of the divertor into the upstream scrape of layer region. The 6th and 7th ionization stages N^{6+} and N^{7+} of Nitrogen are located more and more also in the confined core region. For the highest ionization stage N^{7+} one can observe a very subtle density increase ($\sim$ 20–30 %) spread around the outer midplane originating from the magnetic mirror in this region. In the simulations with the old simplified Coulomb collision model [4], which was only based on an energy relaxation time and was neglecting any scattering of the kinetic ions, we observed huge un-physical N^{5+} and N^{7+} density blobs (factor 5–8 higher density) in the magnetic mirror regions at the high field side of the X-point and at the outer midplane. This exaggerated trapping in the magnetic mirror is now gone, as we have now with the improved Coulomb collision operator included the pitch-angle scattering of the kinetic ions into the loss cone of the magnetic mirror correctly.

5. Comparison of EMC3-EIRENE KIT to ERO2.0

As a next step, we now wish to benchmark the transport of the EMC3-EIRENE kinetic ion transport module KIT against the well-established ERO2.0 code. The full orbit code ERO2.0 has also the possibility to do simulations in the guiding centre approximation with the same Coulomb collision operator [8] we have implemented now into the EMC3-EIRENE code. So, both codes have the same physical transport model available which facilitates the comparison between them.

As a plasma background we use the same ITER medium density L-mode scenario as in the previous section. To avoid any influence from differences in the surface models of the codes, we will use a non-recycling impurity like Beryllium for the benchmark (all walls are fully absorbing). To have a well-defined source, we will puff mono-energetic (25 eV) Beryllium atoms with a δ-velocity-distribution at the outer midplane $(R, Z, \varphi) = (8.2\ \text{m},\ 0\ \text{m},\ 0^{\circ})$ in negative R-direction with a puff strength of $\Gamma_{Be} = 1 \times 10^{19}$ atoms/s. The simulation volume is a 40° toroidal section (from $\varphi = -20^{\circ} \cdots +20^{\circ}$) with periodic toroidal boundary conditions (which corresponds to 9 equally toroidally distributed puff location in the full 360° torus). At the inner core boundary of the simulation volume, we use in both codes reflecting boundary conditions.

In Fig. 3 we see the total Beryllium density (sum over all ionization stages) at $\varphi = 0^{\circ}$ obtained by the ERO2.0 code on the left side and for the EMC3-EIRENE kinetic ion transport module on the right side. The density blob at the outer midplane at $Z = 0$ m is produced by the Beryllium puff. Due to the parallel transport, the density blob forms a tube in positive and negative toroidal direction and, due to the 40° toroidal symmetry, cuts the $\varphi = 0^{\circ}$ toroidal plane again at $Z \approx \pm 1.9$ m. The density tube continues further in parallel and anti-parallel direction and forms the poloidal structure of density blobs by cutting the $\varphi = 0^{\circ}$ toroidal plane on and on. The Beryllium density structures formed by both codes are very similar and one can only observe a slight difference in the logarithmic density scaling towards the core boundary surface where the EMC3-EIRENE code seems to produce a slightly higher density.

This is more obvious in Fig. 4 where radial density profiles of the individual Beryllium ionization stages obtained by both codes are shown in a linear scaling. The radial density profiles start at the core boundary and go outwards (with increasing s) through the middle of the density blob located at $Z \approx -1.9$ m. The location of the radial profile is indicated in the left plot of Fig. 3 by the blue arrow. The results for the ERO2.0 code are shown in solid lines and for the EMC3-EIRENE kinetic ion transport module in dashed lines. For both codes, practically all Be^{1+} ions (up to Monte-Carlo noise level) are already ionized into the second ionization stage. The density profiles and locations of the peaks for the $Be^{2+} - Be^{4+}$ ionization stages simulated by the ERO2.0 code and EMC3-EIRENE kinetic ion transport module are very close to each other. This indicates that also the kinetic ion transport is very similar in both codes. The main difference we can observe is a 60% higher density obtained by the EMC3-EIRENE kinetic ion transport module for Be^{4+} towards the inner core boundary (small s). We currently speculate that this originates from a slightly different implementation of the reflecting boundary condition at the core surface in both codes. But this need and will be investigated further together with more detailed benchmarks between the ERO2.0 code and the EMC3-EIRENE kinetic ion transport module outside the scope of this publication.

6. Conclusions

We have implemented a new improved Coulomb collision module in the EMC3-EIRENE kinetic ion transport module which treats the scattering of the kinetic ions correctly and avoids the excessive, un-physical confinement of the kinetic ions in the magnetic mirror regions observed with the old simplified Coulomb collision module of EIRENE [4]. It turned out that a small enough time-step for the Coulomb collision

module is crucial to avoid divergence. This was achieved by either simply choosing the time-step as a small fraction (10^{-4}) of the Spitzer slowing down time τ_s or by the implementation of an adaptive time-step control with error estimate which turned out to be about ten times faster. This led to a reasonable solution for the simulation of Nitrogen seeding into a medium density ITER L-mode scenario. To check the correctness of the EMC3-EIRENE kinetic ion transport module, we benchmarked the code against the well-established ERO2.0 code. For this we used the non-recycling species Beryllium to avoid any influence from differences in the surface models of the codes. In this comparison we achieved good agreement between both codes, even though we observed about 60% higher Be^{4+} density at the core boundary with the EMC3-EIRENE kinetic ion transport module compared to ERO2.0. This disagreement together with more detailed code-code comparisons will be investigated in future works as well as improving further the new Coulomb collision model by adding thermal force effects.

CRediT authorship contribution statement

D. Harting: Writing – original draft, Visualization, Validation, Software, Methodology, Investigation, Funding acquisition, Formal analysis, Conceptualization. **D. Reiser:** Writing – review & editing, Validation, Supervision, Resources, Methodology, Conceptualization. **S. Rode:** Resources, Methodology, Data curation. **J. Romazanov:** Visualization, Validation, Software, Resources, Methodology. **P. Börner:** Software, Resources, Data curation. **Y. Feng:** Software, Resources, Data curation. **H. Frerichs:** Software, Resources, Data curation. **A. Knieps:** Software, Resources, Investigation.

Declaration of competing interest

The authors declare the following financial interests/personal relationships which may be considered as potential competing interests: Derek Harting reports was provided by EUROFusion. Derek Harting reports a relationship with EUROFusion that includes: funding grants.

Acknowledgements

The authors gratefully acknowledge the computing time granted through JARA on the supercomputer JURECA [15] at Forschungszentrum Jülich.

This work has been carried out within the framework of the EUROfusion Consortium, funded by the European Union via the Euratom Research and Training Programme (Grant Agreement No 101052200 - EUROfusion). Views and opinions expressed are however those of the author(s) only and do not necessarily reflect those of the European Union or the European Commission. Neither the European Union nor the European Commission can be held responsible for them.

Data availability

The authors do not have permission to share data.

References

[1] Y. Feng, F. Sardei, J. Kisslinger, 3D fluid modelling of the edge plasma by means of a monte carlo technique, J. Nucl. Mater. 266–269 (1999) 812–818, https://doi.org/10.1016/S0022-3115(98)00844-7.
[2] Y. Feng, H. Frerichs, M. Kobayashi, A. Bader, F. Effenberg, D. Harting, H. Hoelbe, J. Huang, G. Kawamura, J.D. Lore, T. Lunt, D. Reiter, O. Schmitz, D. Sharma, Recent improvements in the EMC3-eirene code, Contrib. Plasma Phys. 54 (4–6) (2014) 426–431, https://doi.org/10.1002/ctpp.201410092.
[3] D. Reiter, M. Baelmans, P. Boerner, The EIRENE and B2-EIRENE codes, Fusion Sci. Technol. 47 (2) (2005) 172–186, https://doi.org/10.13182/FST47-172.
[4] D. Harting, A. Knieps, D. Reiser, S. Rode, J. Romazanov, P. Börner, Y. Feng, H. Frerichs, Refined guiding centre approximation for kinetic studies of Nitrogen seeding in medium density ITER L-mode scenarios with EMC3-EIRENE, NME 33 (2022) 101279, https://doi.org/10.1016/j.nme.2022.101279.
[5] D. Reiser, D. Reiter, M.Z. Tokar, Improved kinetic test particle model for impurity transport in tokamaks, Nucl. Fusion 1998 **38** 165 doi: 10.1088/0029-5515/38/2/302.
[6] K. Särkimäki, E. Hirvijoki, J. Terävä, Adaptive time-stepping Monte Carlo integration of Coulomb collisions, *CPC* 222 (2018) 374–383, https://doi.org/10.1016/j.cpc.2017.09.025.
[7] H. Lamba, An adaptive timestepping algorithm for stochastic differential equations, J. Comput. Appl. Math. 161 (2) (2003) 417–430, https://doi.org/10.1016/j.cam.2003.05.001.
[8] S. Rode, J. Romazanov, D. Reiser, S. Brezinsek, C. Linsmeier, A. Pukhov, Implementation and validation of guiding centre approximation into ERO2.0, Contrib. Plasma Phys. e202100172 (2022), https://doi.org/10.1002/ctpp.202100172.
[9] K. Nanbu, Theory of cumulative small-angle collisions in plasmas, PhysRevE 55 (1997) 4642, https://doi.org/10.1103/PhysRevE.55.4642.
[10] A.M. Dimits, C. Wang, R. Caflisch, B.I. Cohen, Y. Huang, Understanding the accuracy of Nanbu's numerical Coulomb collision operator, J. Comput. Phys. 228 (2009) 4881–4892, https://doi.org/10.1016/j.jcp.2009.03.041.
[11] G. Ciraolo, H. Bufferand, P. Di Cintio, P. Ghendrih, S. Lepri, R. Livi, Y. Marandet, E. Serre, P. Tamain, M. Valentinuzzi, Fluid and kinetic modelling for non-local heat transport in magnetic fusion devices, Contrib. Plasma Phys. 58 (2018) 457–464, https://doi.org/10.1002/ctpp.201700222.
[12] N.G. van Kampen, Itô Versus Stratonovich, J. Stat. Phys. 24 (1981) 175–187, https://doi.org/10.1007/BF01007642.
[13] H.P. Summers, (2004) The ADAS User Manual, version 2.6 http://www.adas.ac.uk.
[14] AMJUEL database http://www.eirene.de.
[15] Jülich Supercomputing Centre, JURECA: Modular supercomputer at Jülich Supercomputing Centre, J. Large-Scale Res. Facilities 4 (2018) A132. https://doi.org/10.17815/jlsrf-4-121-1.